Available online at website: https://journal.bcrec.id/index.php/bcrec

Bulletin of Chemical Reaction Engineering & Catalysis, 20 (3) 2025, 471-482

Original Research Article

Eco-Friendly Photocatalyst from Limestone: ZnO-Hydroxyapatite Composite for Efficient Rhodamine B Removal

I Nyoman Sukarta[1,4,*], I Wayan Budiarsa Suyasa[2], I Gede Mahardika[3], Iryanti Eka Suprihatin[2], I Dewa Ketut Sastrawidana[1], I Gusti Lanang Wiratma[1], Dewa Komang Darmayasa[1]

[1]Chemistry Department, Faculty of Mathematics and Natural Sciences, Universitas Pendidikan Ganesha, Jl. Udayana Singaraja, Bali 81117, Indonesia.
[2]Chemistry Department, Faculty of Mathematics and Natural Sciences, Udayana University, Jimbaran, Badung Bali 80361, Indonesia.
[3]Animal Husbandry Department, Faculty of Animal Husbandry, Udayana University, Jimbaran, Badung Bali 80361, Indonesia.
[4]Environmental Science Doctoral Program, Udayana University, Jl. PB. Sudirman Denpasar, Bali, Indonesia.

Received: 15th June 2025; Revised: 20th July 2025; Accepted: 22th July 2025
Available online: 25th July 2025; Published regularly: October 2025

Abstract

This study aims to synthesize and characterize a limestone-based ZnO-hydroxyapatite (HA/ZnO) composite and evaluate its performance in the photocatalytic degradation of Rhodamine B under UV irradiation. Hydroxyapatite was synthesized by reacting calcined CaO from limestone with orthophosphoric acid and subsequently combined with ZnO via a co-precipitation–hydrothermal method. The materials were characterized using X-ray Diffraction (XRD) and Fourier Transform Infra Red (FTIR) to determine their crystal structure and functional groups. The HA/ZnO composite exhibited the smallest crystallite size (14.86 nm), indicating enhanced surface area and strong interfacial interaction. Photodegradation tests revealed optimal conditions at pH of 9, Rhodamine B concentration of 20 mg/L, and catalyst dosage of 1.5 g, achieving a maximum degradation efficiency of 99.81%. Toxicity assessment using a corn seed germination test showed a significant increase in germination rate from 16% (untreated) to 92% (after photocatalytic treatment). These findings suggest that the limestone-derived HA/ZnO composite is a promising, environmentally friendly, and efficient photocatalyst for textile dye wastewater treatment.

Keywords: Photodegradation; ZnO-hydroxyapatite; limestone; Rhodamine B; photocatalyst

How to Cite: Sukarta, I. N., Suyasa, I. W. B., Mahardika, I. G., Suprihatin, I. E., Sastrawidana, I. D. K., Wiratma, I. G. L., Darmayasa, D. K. (2025). Eco-Friendly Photocatalyst from Limestone: ZnO-Hydroxyapatite Composite for Efficient Rhodamine B Removal. *Bulletin of Chemical Reaction Engineering & Catalysis*, 20 (3), 471-482. (doi: 10.9767/bcrec.20426)

Permalink/DOI: https://doi.org/10.9767/bcrec.20426

1. Introduction

The textile industry plays an important role in national development, absorbing 20 percent of the total workforce in the processing industry. However, in addition to having a positive impact on the economy, the development of the textile industry also has the potential to damage the environment. The textile industry is one of the industries that uses a lot of chemicals and water in its production process. Textile wastewater contains high organic and inorganic contaminants with extreme color intensity resulting from the use of large amounts of chemicals including dyes in the textile dyeing process [1,2]. One of the dyes widely used in textile dyeing is rhodamine B. It is estimated that more than 100,000 tons of synthetic dyes per year are consumed for the textile industry and around 10-50% is discharged into the environment as wastewater [3].

* Corresponding Author.
Email: nyoman.sukarta@undiksha.ac.id (I.N. Sukarta)

Rhodamine B dye, like other dyes, is stable to light, heat, oxidation, and is not biodegradable [4]. Due to its non-degradable nature and inherent structural stability, Rhodamine B is categorized as a neurotoxic dye in humans and animals, causing infections in the eyes, skin, digestive tract, and respiratory tract [5].

Many methods have been used to degrade hazardous compounds in textile waste. One method that can be used to remove organic pollutants such as textile dye waste is the photocatalysis or photodegradation method [6]. Photocatalysis is generally defined as a chemical reaction process assisted by light and a catalyst. The basic principle of photocatalysis is the irradiation of the catalyst using photons with sufficient energy to produce hydroxyl radicals that break down pollutants [7]. Photocatalysis is a simple and effective method for treating dye wastewater that is very difficult to degrade [8]. Among the various semiconductors, ZnO is one of the catalysts that is widely used for photocatalysis applications because it is effective, inexpensive, and non-toxic for the degradation of various pollutants [9]. ZnO is an environmentally friendly and abundant semiconductor with n-type conductivity and a wide band gap of 3.3 eV [10]. The advantage of ZnO as a photocatalyst is that it has the same band gap energy but shows higher absorption efficiency in most of the solar spectrum when compared to TiO_2 [11]. It is also reported that among various semiconductors, ZnO has higher efficiency in the photocatalytic degradation of some organic dyes than TiO_2 [12].

However, ZnO as a photocatalyst still has several weaknesses such as low adsorption capacity in absorbing substances to be degraded, rapid recombination of electron-hole pairs produced by photogeneration, thus reducing its photocatalytic effectiveness, and easy to aggregate or clump when used directly as a photocatalyst in the photocatalytic process. To overcome this problem, research activities have developed to strengthen ZnO photocatalysts by manipulating their nanostructure and morphology, one of which is combining foreign materials (metal/metal oxide, ceramics, or polymers) in ZnO semiconductors in the form of composites.

Hydroxyapatite ($Ca_{10}(PO_4)_6(OH)_2$) is a calcium phosphate bioceramic and biomaterial that is highly sought after in various fields due to its extraordinary structure and inherent properties such as its large adsorption capacity, acid-base adjustment ability, ion exchange ability, and good thermal stability. Research on hydroxyapatite has been widely conducted due to its very broad applications in various fields including in the environmental field or waste treatment as an adsorbent, catalyst support in the photodegradation process.

Considering the inherent properties and potential of both materials, the integration of ZnO and hydroxyapatite into a composite structure is expected to overcome the limitations of ZnO as a photocatalyst. A composite is a hybrid material composed of two or more distinct components with different physical and chemical characteristics, designed to produce synergistic properties superior to those of the individual constituents [13]. Hydroxyapatite offers high adsorption capacity, thermal stability, and ion exchange ability, while ZnO is an efficient and widely used photocatalyst for the degradation of various organic dyes. The combination of these materials in a composite system provides several advantages over the use of either component alone. These include enhanced photocatalytic efficiency due to improved UV light absorption and extended charge carrier (electron–hole pair) lifetime, which contribute to more effective degradation reactions. Furthermore, hydroxyapatite provides additional surface area that facilitates greater adsorption of dye molecules and organic pollutants, thereby accelerating the degradation process. Importantly, hydroxyapatite acts as a structural matrix that prevents ZnO agglomeration, maintaining the optimal surface area of ZnO necessary for efficient photocatalytic activity[14]. However, previous studies have rarely reported the use of hydroxyapatite derived from calcined limestone—a highly abundant and inexpensive material—as a support matrix for ZnO in photocatalytic applications. In addition, limited attention has been given to the environmental safety of the photocatalytic process, particularly regarding the toxicity of Rhodamine B degradation by-products. This presents a research gap in developing low-cost, sustainable composites while ensuring their environmental viability through toxicity evaluation. The novelty of this study lies in the synthesis of ZnO-hydroxyapatite composites using limestone-based HA, combined with a comprehensive assessment of structural characteristics and toxicity. This dual approach offers scientific merit by advancing both materials engineering and environmental risk assessment in photocatalytic wastewater treatment.

Based on this background, the present study focuses on the synthesis and characterization of limestone-derived hydroxyapatite as a ZnO-supporting catalyst for the photocatalytic degradation of Rhodamine B dye. Although hydroxyapatite is naturally available in sources such as apatite minerals, bones, and animal teeth, its use is limited due to the presence of impurities and lack of control over material morphology and structure. Naturally derived hydroxyapatite generally requires complex and costly purification processes to meet functional standards [15].

Therefore, synthetic hydroxyapatite offers a practical alternative, enabling controlled structure, improved purity, and customizable properties for more efficient application in environmental and photocatalytic systems.

In photocatalytic applications, material structure plays a critical role in determining catalytic efficiency. Thus, the structures of hydroxyapatite, ZnO, and ZnO-hydroxyapatite composites were investigated, as the physicochemical properties of materials significantly influence their performance in photodegradation processes. Additionally, a toxicity assessment of the Rhodamine B degradation products was conducted to ensure environmental safety. Although photocatalysis aims to break down pollutants into simpler compounds, the formation of intermediate by-products may still pose toxic risks. Therefore, toxicity evaluation is essential to determine the environmental viability of photocatalyst use in wastewater treatment.

2. Materials and Method

2.1 Materials

For the synthesis of hydroxyapatite (HA) and the HA/ZnO composite, analytical-grade reagents including orthophosphoric acid (H_3PO_4), zinc oxide (ZnO), and ammonia (NH_3) were used, all procured from Sigma-Aldrich. Limestone obtained from Bali served as a natural source of calcium carbonate ($CaCO_3$), which was calcined to produce calcium oxide, used as a precursor alongside H_3PO_4. Ammonia was employed to adjust the pH of the reaction medium during synthesis. The chemical structure of Rhodamine B used in the photocatalytic degradation experiments is illustrated in Figure 1.

2.2. Synthesis of HA/ZnO Nanocomposites

The HA/ZnO nanocomposite was synthesized using co-precipitation and hydrothermal methods, both of which are known to yield materials with high crystallinity and homogeneous particle distribution [16]. The process began with the calcination of limestone at 1000 °C to convert $CaCO_3$ into CaO, which was then reacted with phosphoric acid to form hydroxyapatite [17]. The resulting hydroxyapatite was combined with ZnO through either impregnation or co-precipitation, followed by further calcination at 1000 °C to produce a highly crystalline nanocomposite. Material characterization was performed using X-ray diffraction (XRD) and Fourier-transform infrared spectroscopy (FTIR).

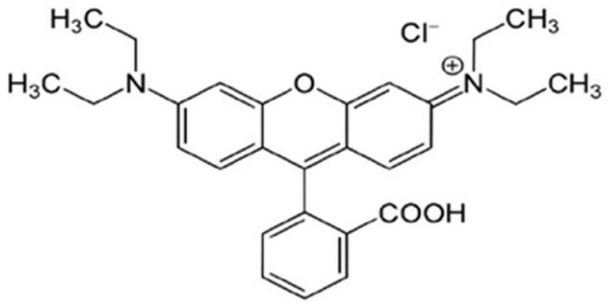

Figure 1. Molecular structure of Rhodamine B.

2.3. Photocatalytic degradation of Rhodamine B Dye

A 25-Watt UV lamp was employed as the photon energy source for the photocatalytic degradation of Rhodamine B. To maintain homogeneous electrolyte distribution, 500 mL of Rhodamine B solution at a concentration of 50 mg/L was added into the photocatalytic reactor and continuously stirred at 150 rpm using an automatic magnetic stirrer. At 120 minute intervals, a 15 mL sample was withdrawn. After separating the suspended particles, the absorbance was measured at a wavelength of 554 nm. The degradation efficiency of Rhodamine B via photocatalytic and adsorption processes was investigated at various weight ratios of HA/ZnO. The degradation efficiency was calculated using the following equation:

$$DP(\%) = \frac{(A_1 - A_2)}{A_1} \times 100\% \quad (1)$$

where, DP is degradation percentage (%), A_1 is the initial absorbance of dye, and A_2 is absorbance of dye after treatment at certain times.

2.4. Test of Rhodamine B Photodegradation Results

The toxicity test of the results of the textile dye decomposition was carried out by germination test according to the AFNOR X31 201 standard, based on the method described by previous researcher [18] with some modifications. The germination test was carried out as follows: a filter paper disc was placed at the bottom of the petri dish, then 20 corn seeds were placed in each dish and the filter paper was irrigated by adding 4 mL of test solution or distilled water as a blank/control. The test solution in question was the rhodamine B dye solution recorded as Rhodamine B0 (RHB0) which means the dye before treatment (without photocatalytic) and Rhodamine B1 (RHB1) which means the dye after photocatalytic treatment. Furthermore, the dish was placed in an incubator for 5 days at a temperature of 25-28 °C and its humidity was maintained. After 5 days, the number of germinated seeds was counted and the germination rate was calculated using the following equation:

$$GR(\%) = \frac{GR}{BG} \times 100\% \quad (2)$$

Where, *GR* is germination rate (%), *GT* is germination test (%), and *BG* is blank germination (%).

3. Results and Discussion

3.1. Synthesis of HA/ZnO Nanocomposites

Calcium carbonate ($CaCO_3$) contained in limestone is around 95% by weight. $CaCO_3$ has the potential to be a source of raw material for hydroxyapatite synthesis. Calcination of limestone to convert $CaCO_3$ into CaO is carried out through the following reaction:

$$CaCO_{3(s)} \xrightarrow{1000\,^{\circ}C} CaO_{(s)} + O_{2(g)} \quad (3)$$

$$CaO_{(s)} + H_2O_{(l)} \longrightarrow Ca(OH)_{2(aq)} \quad (4)$$

$$10Ca(OH)_{2(aq)} + 6H_3PO_{4(aq)} \xrightarrow{pH\ 10-11} Ca_{10}(PO_4)_6(OH)_2(s) + 18H_2O_{(l)} \quad (5)$$

The synthesis of ZnO-hydroxyapatite composite based on limestone was carried out through a multistep chemical transformation process, as illustrated in Figure 2. The initial step involved the calcination of natural limestone at 1000 °C to produce calcium oxide (CaO) (Figure 2b). This CaO was then reacted with water to form calcium hydroxide, $Ca(OH)_2$ (Figure 2c), which served as the main precursor for hydroxyapatite synthesis.

Subsequently, $Ca(OH)_2$ was reacted with orthophosphoric acid (H_3PO_4) under alkaline conditions to form hydroxyapatite [$Ca_{10}(PO_4)_6(OH)_2$] as a fine white powder (Figure 2d). The product exhibited morphology and texture which was consistent with synthetic hydroxyapatite reported in previous studies. In the final step, the hydroxyapatite was combined with ZnO via co-precipitation, followed by a second calcination at high temperature to produce the ZnO-hydroxyapatite composite (Figure 2e). The resulting composite appeared brighter and more homogeneous, indicating uniform dispersion of ZnO within the hydroxyapatite matrix.

This stepwise synthesis demonstrates not only the efficient transformation of limestone into high-purity hydroxyapatite but also the successful incorporation of ZnO into the composite structure. The resulting composite structure plays a crucial role in enhancing the specific surface area and catalytic stability of the material. This synergy is expected to improve the photocatalytic degradation performance against organic pollutants, as further discussed in the following photocatalytic performance section

3.2. XRD Analysis

X-ray diffraction (XRD) analysis was employed to characterize ZnO, hydroxyapatite (HA), and the HA-ZnO composite in order to determine the crystal structure of each sample. The XRD diffractogram results for ZnO, hydroxyapatite, and the HA/ZnO composite are presented in Figure 3. As shown in Figure 3, the XRD pattern for the ZnO sample exhibits distinct diffraction peaks at 2θ values of 31.89°, 34.54°, 36.33°, 47.65°, 56.76°, 63.00°, and 68.10°, indicating the presence of crystalline ZnO. These peaks correspond to the standard JCPDS card no. 01-073-8417, confirming the hexagonal wurtzite structure typical of zinc oxide. The findings are in agreement with [19], who reported similar peaks at 2θ = 31.95°, 34.61°, 36.44°, 47.71°, 56.75°, 63.02°, and up to 77.13°, and are also consistent with [20], who observed sharp peaks at 2θ = 31.7°, 34.4°, 36.2°, 47.5°, 56.6°, and 62.8°. These consistent results confirm that the synthesized

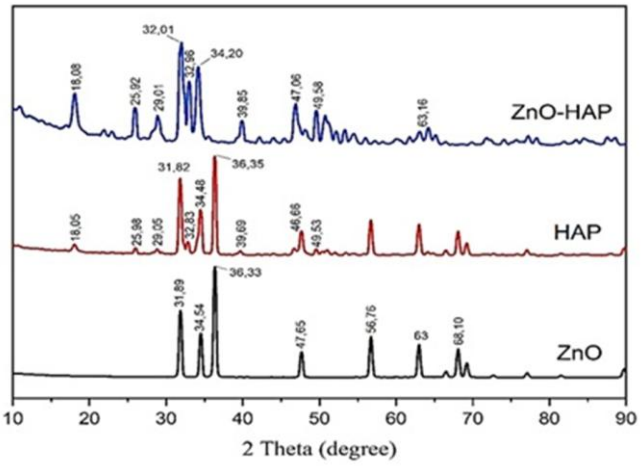

Figure 3. XRD diffractogram of ZnO, HA, and HA/ZnO composite.

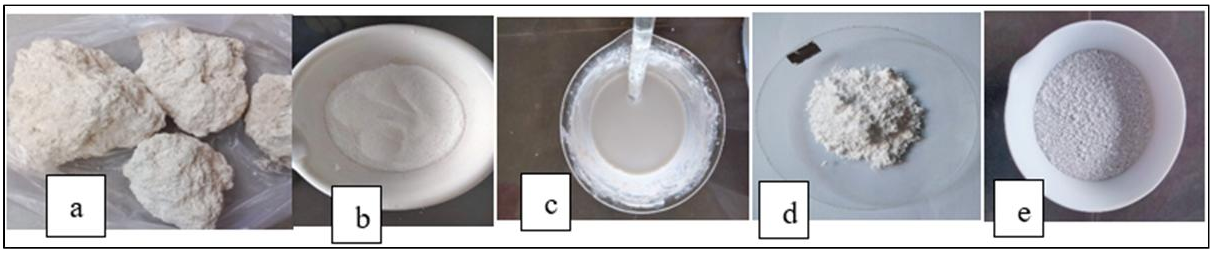

Figure 2. a) Limestone, b) CaO, c) $Ca(OH)_2$, d) hydroxyapatite, e) ZnO-hydroxyapatite.

ZnO exhibits a well-defined crystalline structure, characteristic of standard ZnO [21].

The XRD diffraction pattern of the hydroxyapatite sample revealed characteristic peaks at 2θ angles of 18.05°, 25.98°, 29.05°, 31.82°, 32.83°, 34.48°, 36.35°, 39.69°, 46.66°, and 49.53°. These peaks are consistent with JCPDS card no. 09-0432 for pure hydroxyapatite $Ca_{10}(PO_4)_6(OH)_2$, includes reflections at 2θ = 18.12°, 25.9°, 29.0°, 31.8°, 32.2°, 32.9°, 34.0°, 39.8°, 46.7°, 49.5°, 50.5°, and 53.1° [22]. Based on this pattern, it can be concluded that hydroxyapatite was successfully synthesized via the reaction between $Ca(OH)_2$ and H_3PO_4, as represented by the following equation:

$$10\ Ca(OH)_{2\,(aq)} + 6H_3PO_{4\,(aq)} \rightarrow Ca_{10}(PO_4)_6(OH)_{2(s)} + 18\ H_2O_{(l)} \quad (6)$$

XRD analysis of the HA/ZnO composite revealed diffraction peaks corresponding to ZnO at 2θ = 34.20°, 47.06°, and 63.16°, along with hydroxyapatite peaks at 2θ = 18.08°, 25.92°, 29.01°, 32.01°, 32.96°, 39.85°, and 49.58°. These results confirm that the composite is composed of two primary crystalline phases: ZnO and hydroxyapatite, in agreement with JCPDS reference data. Notably, the diffraction peak at 2θ = 36°, typically associated with ZnO, was no longer observed in the composite pattern, likely due to a significant decrease in intensity or complete suppression. This absence indicates a strong interaction between ZnO and HA during composite formation, suggesting that the process involved more than physical mixing and entailed structural transformation. Such interaction may involve bonding between Zn^{2+} ions and OH^- or PO_4^{3-} groups from hydroxyapatite, resulting in alterations to the original ZnO crystal structure.

The crystallite size of each sample was calculated using the Scherrer equation, as described by Bokuniaeva and Vorokh (2019), and presented in Equation (7):

$$D = \frac{0.9\lambda}{B\cos\theta} \quad (7)$$

where, D is the average crystallite size (nm), λ is the X-ray wavelength for Cu-Kα radiation (0.154 nm), B the full width at half maximum (FWHM) in radians, and θ (theta) is the Bragg angle ranging between 25° and 80°. Based on XRD data analysis, the average crystallite sizes were calculated as 40.18 nm for ZnO, 42.65 nm for hydroxyapatite, and 14.86 nm for the HA/ZnO composite.

The relatively larger crystallite sizes of ZnO and HA indicate higher structural stability but lower specific surface area, which can limit photocatalytic efficiency [23]. In contrast, the smaller crystallite size of the composite suggests strong interaction between ZnO and HA, which suppresses crystal growth, increases structural defects, and enhances surface area. These factors contribute to improved charge transfer and higher photocatalytic activity, making the composite more effective in pollutant degradation applications than either ZnO or hydroxyapatite alone [24,25].

3.3. FTIR Analysis

The results of FTIR analysis for ZnO, HA and HA/ZnO are presented in Figure 4. As shown in Figure 4, the FTIR spectrum of ZnO exhibits an absorption peak at 3731 cm^{-1}, indicating the presence of hydroxyl (OH) groups from adsorbed H_2O molecules. Additionally, the peak at 418 cm^{-1} corresponds to the characteristic vibrational mode of the Zn–O bond, confirming the presence of ZnO in the sample. These findings are consistent with those reported by researcher [26], who observed a peak at 3572 cm^{-1} attributed to hydroxyl (OH) groups and a peak at 412 cm^{-1} corresponding to Zn–O bonding vibrations.

In addition, Zn–O bond vibrations in the low-wavenumber region have been widely reported in the literature. [27] identified a Zn–O stretching vibration peak at 443 cm^{-1}, while additional bands observed at 1630 cm^{-1} and 3446 cm^{-1} were attributed to O–H stretching from adsorbed H_2O molecules. Similar findings were confirmed by [28], who reported absorption bands in the 400–500 cm^{-1} range corresponding to the characteristic stretching mode of Zn–O bonds. Moreover, absorption peaks at 3434 cm^{-1}, 1330 cm^{-1}, and 1670 cm^{-1} were associated with hydroxyl (OH) groups originating from ambient atmospheric moisture.

The FTIR spectrum of the synthesized hydroxyapatite (HA) exhibited characteristic absorption bands representing phosphate (PO_4^{3-}), carbonate (CO_3^{2-}), and hydroxyl (OH^-) groups,

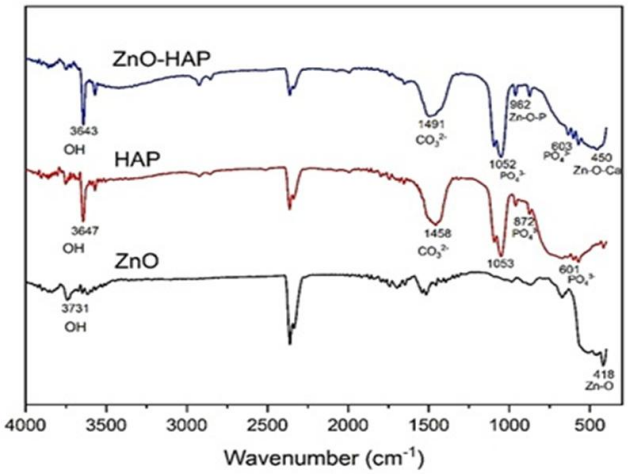

Figure 4. FTIR spectrum of ZnO, HA and HA/ZnO.

which are typical for hydroxyapatite [29,30]. Phosphate group vibrations were observed at wavenumbers 601 cm^{-1}, 872 cm^{-1}, and 1053 cm^{-1}, while the carbonate vibration appeared at 1458 cm^{-1}. The hydroxyl group vibration was detected at 3647 cm^{-1} [31]. These results are consistent with previous studies reporting hydroxyl absorption bands within 3700–2500 cm^{-1} [32], carbonate vibrations between 1428 and 1459 cm^{-1}, and phosphate peaks at 600 cm^{-1}, 958 cm^{-1}, and 1037 cm^{-1} [32]. Furthermore, these findings align with the absorption bands observed in FTIR spectra of commercial hydroxyapatite, where phosphate (PO_4^{3-}) vibrations occur at 964 cm^{-1} and within the 1000–1156 cm^{-1} range, and hydroxyl (OH^-) vibrations are present between 2600 and 3800 cm^{-1}.

The FTIR analysis revealed the presence of a carbonate peak detected at a wavenumber of approximately 1458 cm^{-1}. This peak indicates the presence of carbonate impurities in the synthesized hydroxyapatite (HA) sample. The presence of carbonate may be attributed to several factors, including contamination by carbon dioxide (CO_2) from the air during synthesis or storage, or residual raw materials such as calcium carbonate ($CaCO_3$) that have not fully reacted to form HA. To address this issue, stricter control of the synthesis process and the use of higher purity raw materials are required in future studies.

Based on the FTIR spectrum of hydroxyapatite shown in Figure 3, phosphate groups were detected at three absorption bands. This result indicates that the synthesized hydroxyapatite possesses a high degree of purity. Furthermore, the PO_4^{3-} and OH^- groups appeared with relatively sharp peaks, indicating high absorption intensity. The peak corresponding to the PO_4^{3-} group, the better the crystallinity formed, which implies higher quality hydroxyapatite [33].

In the HA/ZnO composite, the FTIR spectrum closely resembles that of pure hydroxyapatite but shows slight shifts in peak positions and intensities reflecting interactions between ZnO and hydroxyapatite within the composite. These interactions include bonds between Zn^{2+} ions and phosphate groups PO_4^{3-} (Zn–O–P) as well as bonds between Zn^{2+} and Ca^{2+} ions (Zn–O–Ca). The composite spectrum exhibited absorption peaks at 603 cm^{-1} and 1052 cm^{-1} associated with phosphate group vibrations (PO_4^{3-}). The absorption peak at 1491 cm^{-1} corresponds to carbonate groups (CO_3^{2-}), while the peak at 3643 cm^{-1} indicates the presence of hydroxyl groups (OH^-). Peaks at 962 cm^{-1} and 450 cm^{-1} are characteristic of the formation of ZnO–Hydroxyapatite composites, specifically Zn–O–P and Zn–O–Ca bonds. This is supported by previous reports stating that the phosphate (P–O) group in hydroxyapatite exhibits a peak near 960 cm^{-1} that may shift or change intensity due to doping or interaction with Zn ions [34]. Peaks in the low wavenumber region (400–500 cm^{-1}) are typically attributed to Zn–O stretching vibrations interacting with other metal ions, including Ca from hydroxyapatite [35]. The presence of this peak indicates an interaction between ZnO and Ca within the composite, albeit with low intensity, which may suggest that the interaction is not dominant or only a fraction of ZnO forms bonds with Ca [36].

3.4. Photocatalytic Degradation of Rhodamine B Dye

3.4.1. Effect of pH

The effect of pH on the percentage of photocatalytic degradation was investigated at different pH values (4, 7, and 9), while maintaining a constant Rhodamine B dye concentration of 100 mg/L, using 1 gram of the HA/ZnO composite, and an irradiation time of 120 minutes. The purpose of varying the pH was to evaluate the role of acidity or alkalinity conditions on the photocatalytic degradation efficiency. The effect of pH on the degradation efficiency of rhodamine B by the HA/ZnO composite is presented in Figure 5. As shown in Figure 5, the degradation efficiency increased with rising pH of the dye solution. The degradation percentages of rhodamine B at pH of 4, 7, and 9 were 85.49%, 88.72%, and 91.96%, respectively. This phenomenon can be explained by the cationic nature of rhodamine B, where the surface charge of the photocatalyst and the solution pH play a crucial role in the adsorption and photocatalytic degradation processes [37]. At low pH, the catalyst surface tends to be positively charged due to protonation, which leads to electrostatic repulsion between the catalyst surface and rhodamine B molecules (RhB^+), thereby reducing the adsorption of rhodamine B. Additionally, the high concentration of H^+ ions at low pH competes

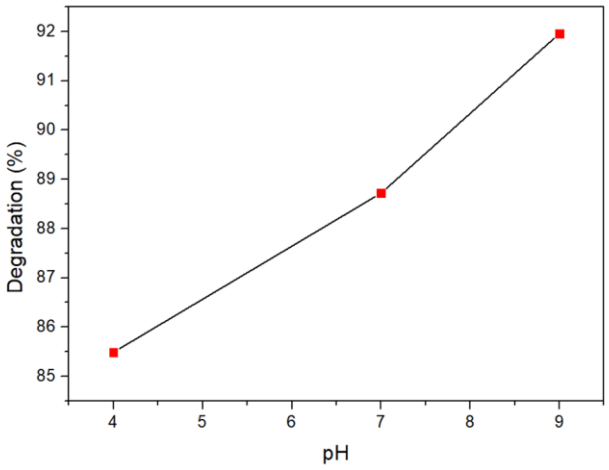

Figure 5. Effect of pH on the percentage of rhodamine B degradation.

with rhodamine B for reaction with hydroxyl radicals (•OH), and the low availability of OH^- ions under acidic conditions limits the formation of these radicals. Consequently, fewer •OH radicals are generated, leading to lower degradation efficiency.

However, at higher pH values, the catalyst surface becomes negatively charged due to deprotonation. This leads to electrostatic attraction between the negatively charged catalyst surface and the positively charged rhodamine B molecules (RhB^+), thereby enhancing the adsorption of rhodamine B onto the catalyst surface. Moreover, under alkaline conditions, the abundant OH^- ions in the solution facilitate the generation of hydroxyl radicals (•OH), which are the primary oxidative species responsible for the photocatalytic degradation process [38]. This combination of increased adsorption and enhanced •OH radical formation contributes to the overall improvement in degradation efficiency [39].

Rhodamine B is a cationic dye, and under alkaline conditions, the photocatalytic degradation efficiency tends to increase. This is attributed to the higher concentration of OH^- ions, which does not only enhance electrostatic interactions between the dye molecules and the catalyst surface but also promotes the formation of hydroxyl radicals (•OH) that serve as the primary oxidative species in the degradation process [37]. This result is consistent with the findings of other researcher group [40], who reported that the optimal degradation percentage of rhodamine B by ZnO occurred at pH of 9, while the lowest degradation was observed at pH of 5. The low degradation efficiency at acidic pH may be due to electrostatic repulsion between the protonated catalyst surface and the positively charged rhodamine B (RhB^+) molecules. Conversely, the increase in degradation efficiency at higher pH is likely associated with the deprotonation of RhB^+, leading to the formation of zwitterionic species that are more readily adsorbed onto the catalyst surface. However, at pH values above 9, the degradation efficiency decreases, possibly due to excess OH^- ions saturating the catalyst surface and creating a negatively charged layer that inhibits interaction with the dye molecules. Therefore, the optimal pH for rhodamine B photocatalytic degradation is pH of 9.

3.4.2. Effect of Rhodamine B concentration.

The concentration of pollutants plays a major role in the photocatalytic degradation of organic contaminants. To investigate the effect of initial dye concentration on the photocatalytic activity of the ZnO–Hydroxyapatite composite, a series of experiments were conducted by adding 1 gram of catalyst (kept constant) into rhodamine B solutions with varying initial concentrations of 20, 40, 60, 80, and 100 mg/L. All experiments were carried out at the previously determined optimal pH of 9 and irradiated for 120 minutes. The graph illustrating the effect of varying initial dye concentrations on the percentage degradation of rhodamine B is presented in Figure 6.

As shown in Figure 6, the degradation percentage of rhodamine B decreases with increasing initial dye concentration. The degradation efficiencies at 20, 40, 60, 80, and 100 mg/L were 96.18%, 94.98%, 93.84%, 92.94%, and 91.96%, respectively. This decline is attributed to the increased number of dye molecules adsorbed onto the catalyst surface, which limits the availability of active sites and reduces the light penetration needed to generate reactive species. This result is consistent with the findings of other researcher group [41], who reported that the degradation efficiency of rhodamine B using ZnO decreased exponentially with increasing initial dye concentration. In their study, maximum degradation efficiency of 63% was observed at 10 mg/L rhodamine B, which dropped to 19% at higher concentrations. This reduction in degradation efficiency is associated with the fact that higher dye concentrations lead to increased solution turbidity and color intensity, hindering light penetration. Consequently, fewer photons reach the catalyst surface, limiting the generation of hydroxyl (•OH) and superoxide (O_2•$^-$) radicals, which are essential for the photocatalytic degradation process, thus resulting in decreased overall degradation efficiency [42,43].

This result is also in agreement with the findings of researcher [44], who reported that the degradation percentage of methylene blue using ZnO–Chitosan composites decreased with increasing dye concentration. The highest decolorization percentage was observed at the

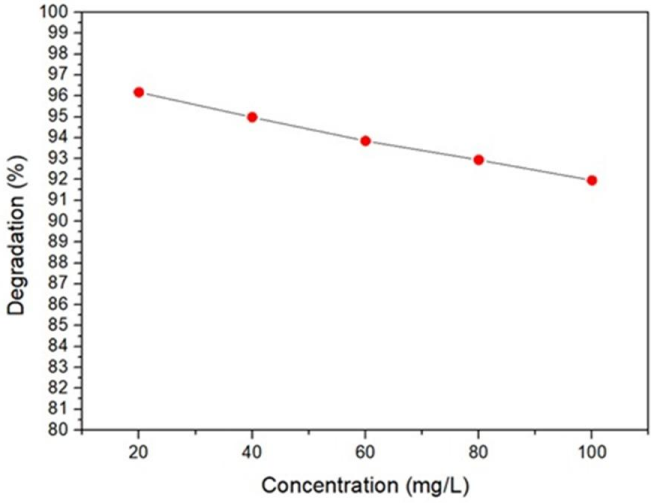

Figure 6. Relationship between dye concentration

lowest concentration of 5 mg/L. At higher concentrations, the number of methylene blue molecules increases, leading to greater competition among the molecules for interaction with active catalytic sites, thereby reducing the likelihood of degradation. Moreover, high dye concentration affects light penetration into the solution. As the solution becomes more concentrated, less light (photons) reaches the catalyst surface, limiting the energy required for the excitation of electrons from the valence band to the conduction band. Consequently, fewer hydroxyl radicals (•OH) are generated, and only a small fraction of methylene blue molecules can be oxidized. Based on the experimental results, the optimal dye concentration for photocatalytic degradation is 20 mg/L.

3.4.3. Effect of HA/ZnO composite mass.

To evaluate the effect of catalyst dosage on dye degradation efficiency, the mass of the HA/ZnO composite was varied at 1 g, 1.5 g, and 2 g in a rhodamine B solution with an optimum concentration of 20 mg/L at pH of 9. The photocatalytic process was carried out for 120 minutes under UV irradiation. This variation aimed to determine the optimum composite mass that yields the highest degradation efficiency. The results of the effect of ZnO–Hydroxyapatite composite dosage variation on the degradation percentage of rhodamine B are presented in Figure 7.

As shown in Figure 7, the degradation percentage increased with the increasing mass of the added composite. The degradation efficiencies at 1 g, 1.5 g, and 2 g of HA/ZnO composite were 96.18%, 99.81%, and 97.91%, respectively. This indicates that the HA/ZnO composite effectively enhanced the photocatalytic degradation of rhodamine B, mainly due to the increased number of active sites on the catalyst surface and the higher generation of reactive species such as hydroxyl radicals (OH•) and superoxide anions (O_2•$^-$), which play a crucial role in the degradation mechanism [45]. However, increasing the catalyst mass beyond 1.5 g led to a slight decline in degradation efficiency. This result aligns with the findings of, who reported that increasing ZnO dosage up to 1 mg/mL improved rhodamine B degradation (10 mg/L at pH 9), but further increases reduced efficiency due to light scattering and decreased photon penetration in the reaction system. Excessive catalyst loading can cause the suspension to become turbid and reduce the light–catalyst interaction, while also potentially inducing particle aggregation, thereby decreasing the available active surface area. Similarly, previous researcher [41] reported that the degradation of rhodamine B with ZnO:Mn increased with catalyst dosage from 0.5 g to 1 g due to the increased availability of active sites and dye adsorption. However, further increases beyond 1 g did not significantly improve degradation because of the "light-shielding effect," where excess catalyst formed a layer that obstructed light penetration, reducing photocatalytic activity [46]. To clarify the involvement of photocatalytic mechanism in the degradation of Rhodamine B, it is essential to consider the role of active species generated during UV-induced excitation of the ZnO-HA composite. Upon UV irradiation, ZnO absorbs photons with energy equal to or greater than its band gap (~3.3 eV), promoting electrons (e^-) from the valence band to the conduction band and leaving behind holes (h^+) in the valence band: ZnO + $h\upsilon \rightarrow e^-$ (CB) + h^+ (VB).

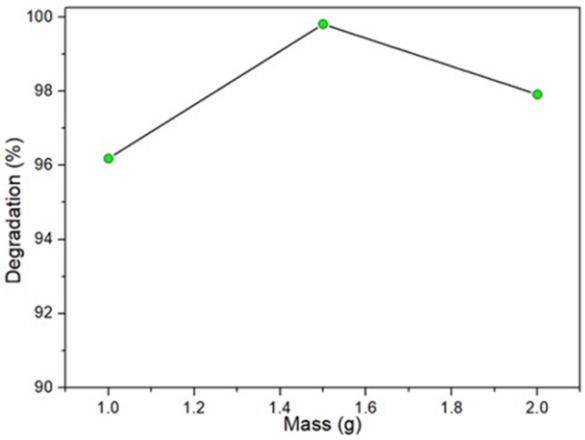

Figure 7. Effect of HA/ZnO composite mass on the degradation power of rhodamine B.

The photogenerated electrons and holes initiate redox reactions at the surface. The conduction band electrons reduce O_2 to form superoxide radicals (•O_2^-), while holes in the valence band oxidize H_2O or OH^- to generate hydroxyl radicals (•OH):

$$O_2 + e^- \rightarrow \cdot O_2^- \quad (8)$$

$$H_2O/OH^- + h^+ \rightarrow \cdot OH \quad (9)$$

These reactive oxygen species (ROS), particularly •OH and •O_2^-, are highly oxidative and play a critical role in breaking down the chromophoric structure of Rhodamine B into less complex, non-toxic compounds. Furthermore, the integration of hydroxyapatite does not only enhance the surface area for dye adsorption but also suppresses the recombination of photoinduced charge carriers by acting as an electron mediator or trap site, thereby improving overall photocatalytic efficiency.

Although the band gap was not directly measured in this study, the use of ZnO as a semiconductor with a known band gap (~3.3 eV) supported its ability to be activated under UV

irradiation and generated ROS necessary for degradation. To better validate the proposed mechanism, future work may involve scavenger studies or electron spin resonance (ESR) analysis to identify dominant reactive species, and UV-Vis diffuse reflectance spectroscopy (DRS) to confirm band gap energy of the composite system.

3.5. Comparison with Previous Studies to Further Support the Photocatalytic

Performance of the ZnO/HA composite synthesized in this study, a comparative analysis with previous works is presented in Table 1. The degradation efficiency of 89% for Rhodamine B under UV irradiation in 120 minutes demonstrates a superior or at least comparable performance to other ZnO-based catalysts. This improvement may be attributed to the enhanced surface interaction and charge separation provided by the limestone-derived hydroxyapatite support.

3.6. Toxicity Test of Textile Dye Decomposition Rhodamine B

A germination assay using corn seeds was conducted to evaluate the toxicity of Rhodamine B before and after photocatalytic degradation (Figure 8). Three types of samples were prepared: untreated Rhodamine B (RHB0), Rhodamine B after photocatalysis (RHB1), and a control using distilled water. Each treatment involved 20 corn seeds placed in petri dishes on moistened filter paper and incubated for 5 days at 25–28 °C. The germination rates were then recorded.

Figure 8. Toxicity test based on corn seed germination using different treatments: Control (distilled water), RHB1 (after photocatalysis), and RHB0 (before treatment).

The relationship graph of the toxicity test of the degradation of textile dye Rhodamine B are presented in Figure 9. As shown in Figure 9, within five days, the germination rate of corn seeds in rhodamine B solution treated with photocatalysis (RHB1) reached 92%. In contrast, the germination rate in the untreated rhodamine B solution (RHB0) was only 16%. This finding is consistent with the study conducted by researcher [26], which evaluated the toxicity of degraded caffeine and rhodamine B solutions through germination assays. After six days, the germination rate of corn seeds in photocatalytically treated caffeine and rhodamine B solutions reached 100%, while in untreated solutions, the germination rates were only 18% for rhodamine B and 23% for caffeine. These results indicate that photocatalytic degradation does not only reduce pollutant concentration but also significantly lowers the toxicity of the resulting by-products. This reduction in toxicity is likely due to the high degree of mineralization achieved during photocatalysis, producing water with low toxicity, potentially safe for agricultural irrigation purposes.

4. Conclusions

This study successfully synthesized and characterized a ZnO-hydroxyapatite (HA) composite derived from limestone using co-precipitation and hydrothermal methods.

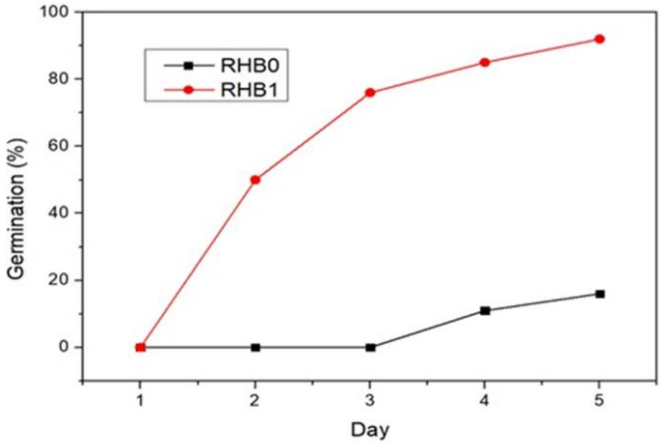

Figure 9. The relationship graph of toxicity test of Rhodamine B solution resulting from photodegradation.

Table 1. Comparison of Rhodamine B degradation efficiency with previous studies.

Photocatalyst	Light Source	Time (min)	Degradation Efficiency (%)	Reference
ZnO nanoparticles	UV	120	78%	[47]
TiO_2	UV	120	73%	[48]
ZnO-Loaded GAC Nanocomposite	UV	120	82%	[49]
ZnO/HA (this work)	UV	120	89%	This study

Structural analysis via XRD and FTIR confirmed the formation of crystalline HA and the integration of ZnO within the composite framework. The composite exhibited a smaller crystallite size (14.86 nm), suggesting enhanced surface area and stronger interfacial interaction between ZnO and HA, which contributed to improved photocatalytic activity. Photocatalytic degradation experiments demonstrated optimal performance under alkaline conditions (pH of 9), at a Rhodamine B concentration of 20 mg/L and catalyst loading of 1.5 g, achieving a maximum degradation efficiency of 99.81%. Toxicity analysis using a germination assay indicated a significant reduction in pollutant toxicity after photocatalytic treatment, with seed germination increasing from 16% (untreated) to 92% (treated solution). Overall, the ZnO-HA composite based on natural limestone offers a promising, low-cost, and environmentally benign alternative for the effective photocatalytic degradation of dye pollutants in textile wastewater. Future work should focus on evaluating the long-term stability, reusability, and degradation performance of the composite under solar light. Additionally, challenges related to process scale-up and continuous-flow operation need to be addressed to assess its feasibility for real-world wastewater treatment applications.

Acknowledgments

The authors would like to thank the Faculty of Mathematics and Natural Sciences Laboratory Center, Ganesha University of Education, for facilitating this work.

CRedit Author Statement

Author Contributions: I Nyoman Sukarta: Conceptualization, Methodology, Formal Analysis, Investigation, Resources, Data Curation, Writing, Visualization, Validation,Review and Editing, I Wayan Budiarsa Suyasa: Conceptualization, Methodology, Formal Analysis, Data Curation, Writting Draft Preparation, Supervision; I Gede Mahardika: Conceptualization, Methodology, Formal Analysis, Supervision; Iryanti Eka Suprihatin: Conceptualization, Methodology, Formal Analysis, Data Curation, Writting Draft Preparation,Writting Draft Preparation, Supervision; I Dewa Ketut Sastrawidana: Conceptualization, Methodology, Formal Analysis, Data Curation, Writting Draft Preparation,Software, Project Administration; I Gusti Lanang Wiratma: Validation, Writing, Review and Editing, Data Curation; Dewa Komang Darmayaa: Data Curation, Visualization, Resources, Review and Editing. All authors have read and agreed to the published version of the manuscript.

References

[1] Sukarta, I.N., Ayuni, N.P.S., Sastrawidana, I. D.K. (2021). Utilization of Khamir (Saccharomyces cerevisiae) as Adsorbent of Remazol Red RB Textile Dyes. *Ecological Engineering & Environmental Technology,* 22(1), 117–123. DOI: 10.12912/27197050/132087.

[2] Sudiana, I.K., Sastrawidana, I.D.K., Sukarta, I.N. (2022). Adsorption Kinetic and Isotherm Studies of Reactive Red B Textile Dye Removal Using Activated Coconut Leaf Stalk. *Ecological Engineering & Environmental Technology,* 23(5), 61–71. DOI: 10.12912/27197050/151628.

[3] Tan, L.S., Jain, K., Rozaini, C.. (2010). Adsorption of Textile Dye from Aqueous Solution on Pretreated Mangrove Bark, An Agricultural Waste: Equilibrium and Kinetic Studies. *Journal of Applied Sciences in Environmental Sanitation,* 5(3).

[4] Tao, P., Xu, Y., Song, C., Yin, Y., Yang, Z., Wen, S. (2017). A novel strategy for the removal of rhodamine B (RhB) dye from wastewater by coal-based carbon membranes coupled with the electric. *Separation and Purification Technology,* 179, 1–23. DOI: 10.1016/j.seppur.2017.02.014.

[5] Hamdaoui, O. (2011). Intensification of the sorption of Rhodamine B from aqueous phase by loquat seeds using ultrasound. *Desalination* 271(1–3), 279–286. DOI: 10.1016/j.desal.2010.12.043.

[6] Carabin, A., Drogui, P., Robert, D. (2015). Photo-degradation of carbamazepine using TiO_2 suspended photocatalysts. *Journal of the Taiwan Institute of Chemical Engineers,* 54, 109–117. DOI: 10.1016/j.jtice.2015.03.006.

[7] Ibhadon, A.O., Fitzpatrick, P. (2013). Heterogeneous Photocatalysis: Recent Advances and Applications. *Catalysts,* 3, 189–218. DOI: 10.3390/catal3010189.

[8] Rafiq, A., Ikram, M., Ali, S., Niaz, F., Khan, M., Khan, Q., Maqbool, M. (2021). Photocatalytic degradation of dyes using semiconductor photocatalysts to clean industrial water pollution. *Journal of Industrial and Engineering Chemistry*. 97, 111–128. DOI: 10.1016/j.jiec.2021.02.017

[9] Lal, M., Sharma, P., Singh, L. Ram, C. (2023). Photocatalytic degradation of hazardous Rhodamine B dye using sol-gel mediated ultrasonic hydrothermal synthesized of ZnO nanoparticles. *Results in Engineering*. 17, 1-13. DOI: 10.1016/j.rineng.2023.100890.

[10] Adeel, M., Saeed, M., Khan, I., Muneer, M., Akram, N. (2021). Synthesis and characterization of Co − ZnO and evaluation of its photocatalytic activity for photodegradation of Methyl Orange. *ACS Omega*, 6, 1426−1435. DOI: 10.1021/acsomega.0c05092.

[11] H. Almohamadi, H., Awad, S.A., Sharma, A.K., Fayzullaev, N., Távara-Aponte, A., Chiguala-Contreras, L., Amari, A., Rodriguez-Benites, C., Tahoon, M.A., Esmaeili, H. (2024). Photocatalytic activity of metal- and non-metal-anchored ZnO and TiO_2 nanocatalysts for advanced photocatalysis: comparative study. *Catayst*s, 14(424), 1-35. DOI: 10.3390/catal14070420.

[12] Lee, H.J., Kim, J.H., Park, S.S., Hong, S.S., Lee, G.D. (2014). Degradation kinetics for photocatalytic reaction of methyl orange over Al-doped ZnO nanoparticles. *Journal of Industrial and Engineering Chemistry*, 25, 1–8, DOI: 10.1016/j.jiec.2014.10.035.

[13] El Bekkali, C., Labrag, J., Oulguidoum, A., Chamkhi, I., Laghzizil, A., Nunzi, J.M., Robert, D., Aurag, J. (2022). Porous ZnO / hydroxyapatite nanomaterials with effective photocatalytic and antibacterial activities for the degradation of antibiotics. *Nanotechnology for Environmental Engineering*, 7(2), 333–341, DOI: 10.1007/s41204-021-00172-7.

[14] Binetruy, C., Michaud, V. (2021). Emerging , hybrid & smart composites. *Functional Composite Materials*, 2(16), 1-2, DOI: 10.1186/s42252-021-00028-y.

[15] Atemni,I., Ouafi, R., Hjouji, K., Mehdaoui, I., Ainane, A., Ainane, T. (2023). Extraction and characterization of natural hydroxyapatite derived from animal bones using the thermal treatment process. *Emergent Mater.,* 6(2), 551-560, DOI: 10.1007/s42247-022-00444-1.

[16] Apostoluk, A., Zhu, Y., Gautier, P., Valette, A., Bluet, J.M., Cornier, T., Masenelli, B., Daniele, S. (2023). Improved visible emission from ZnO nanoparticles synthesized via the Co-precipitation method. *Materials,* 16(15), 5400, DOI: 10.3390/ma16155400.

[17] Malau, N.D. (2021). The effect of calcination time variation on CaO synthesa from limestone. *International Journal of Progressive Sciences and Technologies (IJPSAT),* 25(2), 684–689. DOI: 10.52155/ijpsat.v25.2.2946

[18] Khan, S., Malik, A. (2018). Toxicity evaluation of textile effluents and role of native soil bacterium in biodegradation of a textile dye. *Environmental Science and Pollution Research*, 25, 4446–4458, DOI: 10.1007/s11356-017-0783-7.

[19] Ai, Z., Na, W., Li, J., Huang, Z., Huang, H., Peng, Y., Gao, W., Wang, H. (2024). Enhanced low-temperature CO_2 hydrogenation to methane over Co-Zn oxides catalysts. *Catalysis Letters*, 154 (9) 5255–5269, DOI: 10.1007/s10562-024-04700-3.

[20] Abdelhakim, H. K., El-Sayed, E.R., Rashidi, F.B. (2020). Biosynthesis of zinc oxide nanoparticles with antimicrobial , anticancer , antioxidant and photocatalytic activities by the endophytic Alternaria tenuissima. *Journal of Applied Microbiology*, 128, 1634-1646, DOI: 10.1111/jam.14581.

[21] Lahure, P., Salunke, P., Soliwal, R., Yadav, A., Tripathi, S., Koser, A.A. (2015). X-Ray diffraction study of ZnO nanoparticles. *International Journal of Scientific Research in Physics and Applied Sciences*, 3(1), 32–33.

[22] Rafique, M.M.A. (2018) Hydrothermal processing of phase pure and doped hydroxyapatite and its characterization. *Journal of Encapsulation and Adsorption Sciences,* 8, 18–37, DOI: 10.4236/jeas.2018.81002.

[23] Sharma, J., Vashishtha, M., Shah, D.O. (2014). Crystallite size dependence on structural. *Global Journal of Science Frontier Research: B Chemistry*, 14(5), 19-32.

[24] Zhou, W., Sun, L., Li, K., Tian, S. (2024). Enhanced photocatalytic activity of V_2C MXene-Coupled ZnO porous nanosheets with increased surface area and effective. *Materials*, 17(11), 2529, DOI: 10.3390/ma17112529.

[25] Sarkar, D., Pramanik, J., Samajdar, S. (2025). Applied interfaces charge carrier dynamics in semiconductor – cocatalyst interfaces : influence on photocatalytic activities. *RSC Applied Interfaces*, 2(3), 573–598, 2025, DOI: 10.1039/d5lf00044k.

[26] Tanji, K., Navio, J.A., Martín-Gómez, A.N., Hidalgo, M.C., Jaramillo-Páez, C., Naja, J., Hassoune, H., Kherbeche, A. (2020). Role of Fe (III) in aqueous solution or deposited on ZnO surface in the photoassisted degradation of Rhodamine. *Chemosphere*, 241, 125009, DOI: 10.1016/j.chemosphere.2019.125009.

[27] Jayarambabu, N., Kumari, B.S. (2015). Beneficial role of zinc oxide nanoparticles on green crop production. *International Journal of Multidisciplinary Advanced Research Trends*, 2(1), 275-282.

[28] Kulkarni, S.S. (2015). Optical and structural properties of zinc oxide nanoparticles. *International Journal of Advanced Research in Physical Science (IJARPS)*, 2(1), 14–18.

[29] Cahyaningrum, S.E., Herdyastuty, N., Devina, B., Supangat, D. (2018). synthesis and characterization of hydroxyapatite powder by wet precipitation method synthesis and characterization of hydroxyapatite powder by wet precipitation method. *IOP Conference Series: Materials Science and Engineering*, 1–5. DOI: 10.1088/1757-899X/299/1/012039.

[30] Hossain, M.S., Ahmed, S. (2023). FTIR spectrum analysis to predict the crystalline and amorphous phases of hydroxyapatite : a comparison of vibrational motion to reflection. *The Royal Society of Chemistry*, 13, 14625-14630, DOI: 10.1039/d3ra02580b.

[31] Pettersson, P., Barth, A. (2020). Correlations between the structure and the vibrational spectrum of the phosphate group. Implications for the analysis of an important functional group in phosphoproteins. *The Royal Society of Chemistry,* 10(4715), 4715–4724, DOI: 10.1039/c9ra10366j.

[32] Andrushchenko, V., Benda, L., Bour, P. (2015). Vibrational properties of the phosphate group investigated by molecular dynamics and density functional theory. *The Journal of Physical Chemistry*, 119, 10682–10692, DOI: 10.1021/acs.jpcb.5b05124.

[33] Rosa, A.L., Faris, L.R., Dias, V.P., Pacheco, O.B., Marisso, F.D.P., Rodigues Junior, L.F., Sagrillo, M.R., Rossato, A., Santos, L.L. (2022). Effect of synthesis temperature on crystallinity, morphology and cell viability of nanostructured hydroxyapatite via wet chemical precipitation method. *International Journal of Advances in Medical Biotechnology*, 4(2), 29–33, DOI: 10.52466/ijamb.v5i1.110.

[34] Maggi, L., Friuli, V., Cerea, B., Bruni, G., Berbenni, V., Bini, M. (2024). Physicochemical characterization of hydroxyapatite hybrids with meloxicam for dissolution rate improvement. *Molecules*, 29(2419), 1–18, DOI: 10.3390/molecules29112419.

[35] Babu, K. S., Reddy, A. R., Sujatha, C., Reddy, K.V., Mallika, A.N. (2013). Synthesis and optical characterization of porous ZnO. *Journal of Advanced Ceramics*, 2(3), 260–265, DOI: 10.1007/s40145-013-0069-6.

[36] Chaudhari, A.A., Tupe, U.J., Patil, A.V., Dighavkar, C.G. (2022). Synthesis and characterization of zinc oxide nanoparticles using green synthesis method. *International Journal of Creative Research Thoughts (IJCRT)*, 10(2), 302–309.

[37] Kazeminezhad, I., Sadollahkhani, A. (2016). Influence of pH on the photocatalytic activity of ZnO nanoparticles. *Journal of Materials Science: Materials in Electronics,* 27(25), 4206–4215, DOI: 10.1007/s10854-016-4284-0.

[38] Kuśmierek, K., Fronczyk, J. (2023). Adsorptive removal of Rhodamine B Dye from aqueous solutions using mineral materials as low-cost adsorbents. *Water Air Soil. Pollut.*, 234(531), 1–14, DOI: 10.1007/s11270-023-06511-5.

[39] Chen, Y., Ma, D., He, G., Pan, S. (2024). Effects of pH on the photocatalytic activity and degradation mechanism of Rhodamine B over Fusiform Bi photocatalysts under visible light. *Water*, 16(17), 2389, DOI: 10.3390/w16172389.

[40] Jeevarathinam, M., Asharani, I. V. (2024). Synthesis of CuO, ZnO nanoparticles, and CuO-ZnO nanocomposite for enhanced photocatalytic degradation of Rhodamine B : a comparative study. *Scientific Reports*, 14, 9718, DOI: 10.1038/s41598-024-60008-7.

[41] Muhammad, A.S., Hudu, A. (2022). Photocatalytic degradation of rhodamine B dye using Mn doped ZnO nanoparticles Photocatalytic degradation of rhodamine B dye using Mn doped ZnO nanoparticles. *Applied Journal of Environmental Engineering Science*, 8 (4), 273–285. DOI: 10.48422/IMIST.PRSM/ajees-v8i4.34946

[42] Reza, K.M., Kurny, A., Gulshan,F. (2017). Parameters affecting the photocatalytic degradation of dyes using TiO_2 : a review. *Applied Water Science*, 7(4), 1569–1578, DOI: 10.1007/s13201-015-0367-y.

[43] Haleem, A., Ullah, M., Rehman, S., Shah, A., Farooq, M., Saeed, T., Ullah, I., Li, H. (2024). In-Depth photocatalytic degradation mechanism of the extensively used dyes Malachite Green, Methylene Blue, Congo Red, and Rhodamine B via covalent organic framework-based photocatalysts. *Water*, 16, 1588, DOI: 10.3390/w16111588.

[44] Zango, Z.U., Dennis, J.O., Aljameel, A.I., Usman, F., Ali, M.K.M., Abdulkadir, B.A., Algessair, S., Aldaghri, O.A., Ibnaouf, K.H. (2022). Effective removal of methylene blue from simulated wastewater using ZnO-Chitosan nanocomposites: optimization, kinetics, and isotherm studies. *Molecules*, 27, 4746, DOI: 10.3390/molecules27154746.

[45] Zhu, Z., Guo, F., Xu, Z., Di, X., Zhang, Q. (2020) Photocatalytic degradation of an organophosphorus pesticide using a ZnO/rGO composite. *The Royal Society of Chemistry*, 10, 11929–11938, DOI: 10.1039/d0ra01741h.

[46] Tang, R., Sun, K., Liu, F., Lu, S., Chen, H., Chen, J. (2024). Efficient visible-light driven photocatalytic Cr(VI) reduction on S and O co-doped g-C_3N_4 prepared from 2,5-thiophene dicarboxylic acid based macromolecular precursor. *Research on Chemical Intermediates*, 50(2), 973–988, DOI: 10.1007/s11164-023-05187-0.

[47] Ren, X., Du, Y., Qu, X., Li, Y., Yin, L., Shen, K., Zhang, J., Liu, Y. (2023). Controllable synthesis of ZnO nanoparticles with improved photocatalytic performance for the degradation of Rhodamine B under ultraviolet light irradiation. *Molecules*, 28, 5135, DOI: 10.3390/molecules28135135.

[48] Ahouari, H., Samraoui, Z., Soualah, A., Tayeb, K.B. (2024). Photodegradation of Rhodamine B in aqueous solution using TiO_2 polymorphs : EPR spectroscopy investigation. *Water Air Soil. Pollut.*, 235(25), 1–16, DOI: 10.1007/s11270-023-06822-7.

[49] Obayomi, K.S., Lau, S.Y., Xie, Z., Gray, S.R., Zhang, J. (2024). In-situ hydrothermal fabrication of ZnO-loaded GAC nanocomposite for efficient Rhodamine B Dye removal via synergistic photocatalytic and adsorptive performance. *Nanomaterial*, 14, 1234, DOI: 10.3390/nano14141234.